Available online at www.sciencedirect.com
ScienceDirect
Journal of Solid State Chemistry 180 (2007) 2095–2101
JOURNAL OF SOLID STATE CHEMISTRY
www.elsevier.com/locate/jssc

Hydrothermal synthesis of nickel hydroxide nanostructures in mixed solvents of water and alcohol

Li-Xia Yang[a,b], Ying-Jie Zhu[a,b,*], Hua Tong[a,b], Zhen-Hua Liang[a,b], Liang Li[a,b], Ling Zhang[a,b]

[a]*State Key Laboratory of High Performance Ceramics and Superfine Microstructure, Shanghai Institute of Ceramics, Chinese Academy of Sciences, Shanghai 200050, PR China*
[b]*Graduate School of Chinese Academy of Sciences, PR China*

Received 18 December 2006; received in revised form 23 April 2007; accepted 3 May 2007
Available online 18 May 2007

Abstract

Nickel hydroxide nanosheets and flowers have been hydrothermally synthesized using $Ni(CH_3COO)_2 \cdot 4H_2O$ in mixed solvents of ethylene glycol (EG) or ethanol and deionized water at 200 °C for different time. The phase and morphology of the obtained products can be controlled by adjusting the experimental parameters, including the hydrothermal time and the volume ratio of water to EG or ethanol. The possible reaction mechanism and growth of the nanosheets and nanoflowers are discussed based on the experimental results. Porous nickel oxide nanosheets are obtained by heating nickel hydroxide nanosheets in air at 400 °C. The products were characterized by using various methods including X-ray diffraction (XRD), fourier transform infrared (FTIR), transmission electron microscopy (TEM), selected-area electron diffraction (SAED), field emission scanning electron microscopy (FESEM). The electrochemical property of β-$Ni(OH)_2$ nanosheets was investigated through the cyclic voltammogram (CV) measurement.

Keywords: Nickel hydroxide; Nickel oxide; Nanostructures; Hydrothermal

1. Introduction

Nickel hydroxide ($Ni(OH)_2$) is widely used in many applications from power tools to portable electronics and electric vehicles. There are two polymorphs of $Ni(OH)_2$, which are designated as α-$Ni(OH)_2$ and β-$Ni(OH)_2$, respectively. The α-$Ni(OH)_2$ phase displays a more disorderly and larger interlayer spacing (>7.5 Å) as the interlamellar space contains anions, e.g., nitrate, carbonate, sulfate and water molecules. The hexagonal β-$Ni(OH)_2$ phase is brucite-like and well-oriented $Ni(OH)_2$ layers are perfectly stacked along the *c*-axis with an interlamellar distance of 4.60 Å [1–4].

As an active material of the positive electrode of alkaline rechargeable batteries, the performance of such batteries highly depends on the size, morphology and phase of $Ni(OH)_2$. Considerable work has been focused on the morphology-controllable preparation of $Ni(OH)_2$ and related composite materials [5–8]. Recently, Matsui et al. reported the synthesis of single-crystalline $Ni(OH)_2$ nanorods by the hydrothermal reaction in the cavity of carbon nanotubes prepared in anodic aluminum oxide template [9]. $Ni(OH)_2$ tubes were prepared by a template method and tested as the positive electrode material of alkaline rechargeable batteries [10,11]. Liang et al. prepared single-crystalline $Ni(OH)_2$ nanosheets using $Ni(CH_3COO)_2$ and aqueous ammonia [12]. Ribbon- and board-like $Ni(OH)_2$ were also reported and the board-like nanostructures were helpful in improving the electrochemical performance [13,14]. $Ni(OH)_2$ hollow spheres [15,16] and stacks of pancakes [1] were also reported. These preparation methods usually involve the precipitation of $Ni(OH)_2$ by

*Corresponding author. State Key Laboratory of High Performance Ceramics and Superfine Microstructure, Shanghai Institute of Ceramics, Chinese Academy of Sciences, Shanghai 200050, PR China.
Fax: +86 21 52413122.
E-mail address: y.j.zhu@mail.sic.ac.cn (Y.-J. Zhu).

0022-4596/$ - see front matter © 2007 Elsevier Inc. All rights reserved.
doi:10.1016/j.jssc.2007.05.009

employing an alkaline reagent, such as urea, ammonia and NaOH [9–19]. In some methods the template is needed. It is highly desirable to explore simple and low-cost methods for the large-scale production of $Ni(OH)_2$ nanostructures catering to the large demand of this kind of battery material.

Nickel oxide (NiO) has many applications in various fields, such as catalysis [20], gas sensors [21], battery cathode [22], magnetic materials [23,24] and fuel cell electrodes [25]. Although NiO nanoparticles [26], nanorods/nanowires/nanofibers [27–29], nanosheets [12], nanorings [30], hollow spheres [15,16,31] and worm-like nanoporous NiO [32] were reported, the synthesis of nanoporous nanosheets of NiO is still a big challenge to chemists with an aim to improve the specific surface area and enhance the corresponding performances.

Herein, we report a facile strategy to the synthesis of $Ni(OH)_2$ nanosheets and nanoflowers through the hydrolysis of nickel acetate in the mixed solvents of water and ethylene glycol (EG) or ethanol, which may be scaled up to synthesize $Ni(OH)_2$ without the use of the template and other additives. Both α-$Ni(OH)_2$ and β-$Ni(OH)_2$ can be produced by simply adjusting the hydrothermal time. The morphology transformation process from α-$Ni(OH)_2$ to β-$Ni(OH)_2$ in the solution were systematically investigated. Moreover, NiO nanoporous nanosheets were successfully synthesized by thermal decomposition of the as-synthesized $Ni(OH)_2$ at 400 °C in air.

2. Experimental section

2.1. Synthesis procedure of the samples

In a typical experiment, 0.625 g $Ni(CH_3COO)_2 \cdot 4H_2O$ was dissolved in 24 mL mixed solvents of water and EG (or ethanol) with magnetic stirring to form a homogeneous solution, then was transferred into a Teflon-lined stainless steel autoclave (40 mL capacity), sealed and maintained at 200 °C for a fixed time (0.5–10.5 h). The samples were designated as A1, A2, A3 and A4 when the volume ratio of EG to H_2O was 1:23 for 1, 1.5, 3.5 and 10.5 h, respectively; samples B1 and B2 when the volume ratio of EG to H_2O was 1:1 for 1.5 and 3.5 h, respectively; samples C1, C2 and C3 when EG was used as the only solvent (24 mL) for 3.5, 5.5 and 10.5 h, respectively; samples D1, D2, D3 and D4, when the volume ratio of ethanol to H_2O was 1:1 for 1, 1.5, 3.5 and 10.5 h, respectively. After the autoclave was cooled to room temperature naturally, the product was separated by centrifugation, washed with deionized water and ethanol and finally dried at 60 °C in air. For the preparation of NiO, the obtained $Ni(OH)_2$ was calcined in a tubal oven at 400 °C in air for 2 h. The calcined samples were labeled as samples E1 and E2 by heating the corresponding $Ni(OH)_2$ samples A4 and D4, respectively.

2.2. Characterization of the samples

The as-prepared samples were characterized by X-ray powder diffraction (XRD) with a Rigaku D/max 2550 V X-ray diffractometer with a high-intensity Cu Kα radiation ($\lambda = 1.54178$ Å) and a graphite monochromator. Fourier transform infrared (FTIR) spectra were obtained with a spectrophotometer (Thermo Niocolet, NEXUS). The morphology was studied by a JEOL JSM-6700F field emission scanning electron microscopy (FESEM). The transmission electron microscopy (TEM) micrographs, and selected-area electron diffraction (SAED) patterns were taken on a JEOL JEM-2100F field emission transmission electron microscope with an accelerating voltage of 200 kV. The cyclic voltammetric measurements were performed in a three-compartment electrolysis cell at 25 °C using platinum powder microelectrode with the diameter of 100 μm as the working electrode.

3. Results and discussion

3.1. Phase evolution

The crystal phase and structure information on the products were obtained by XRD measurements. Fig. 1 shows the XRD patterns of samples prepared using nickel acetate in 1 mL EG and 23 mL H_2O at 200 °C for different hydrothermal time. The XRD pattern of the product prepared at 200 °C for 1 h (sample A1, Fig. 1a) shows a mixture of typical layered products. One of the phases is indexed to the (0 0 3), (0 0 6), (0 0 9), (1 0 1) and (1 1 0) planes of α-$Ni(OH)_2$ with well-defined peaks at 0.9421, 0.4731, 0.3169, 0.2690 and 0.1552 nm, and the other has a larger d spacing (1.718 nm) indicated as an asterisk. When the hydrothermal time was prolonged to 1.5 h (sample A2), a predominant well-crystalline brucite-like phase of β-$Ni(OH)_2$ with a hexagonal structure (JCPDS No.74-2075) was formed (Fig. 1b). However, α-$Ni(OH)_2$ as a minor phase with d spacings of 1.512, and 0.7508 nm (labeled as #) was also observed. A single phase of well-crystallized brucite-like β-$Ni(OH)_2$ formed when the hydrothermal time was 3.5 h (sample A3, Fig. 1c). No peaks from the

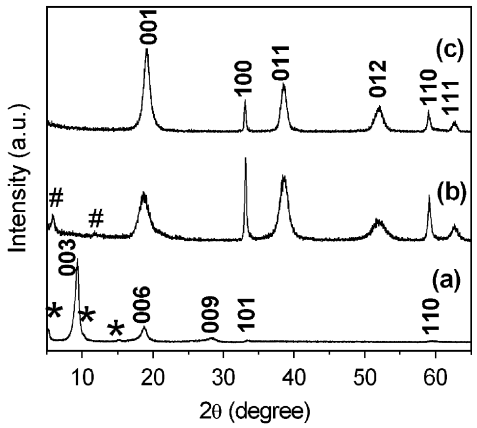

Fig. 1. XRD patterns of samples hydrothermally prepared using $Ni(CH_3COO)_2 \cdot 4H_2O$ in 1 mL EG and 23 mL H_2O at 200 °C for different time. (a) sample A1; (b) sample A2; (c) sample A3.

precursor or intermediates were observed. The expansion of the c parameter of the unit cell of $Ni(OH)_2$ was observed owing to the intercalation of anions. Further evidence for the presence of interlamellar anions and water molecules comes from the FTIR studies and will be discussed later.

Fig. 2 shows the FTIR spectra of different samples. Fig. 2a shows a typical FTIR spectrum of α-$Ni(OH)_2$. The broad band at around 3429 cm^{-1} is characteristic of the stretching vibration of hydroxyl groups hydrogen-bonded to H_2O. The band at about 656 cm^{-1} is due to the δ_{Ni-O-H} vibration [33–36]. The bands observed in the range of 1700-1000 cm^{-1} are attributed to the presence of acetate ions [37]. Fig. 2c shows a typical FTIR spectrum of β-$Ni(OH)_2$. A narrow and sharp peak at 3641 cm^{-1} is owing to the υ_{O-H} stretching vibration, which confirms the brucite structure of β-$Ni(OH)_2$ phase. Peaks at 3444 and 1628 $cm^{-1}$are assigned to the $\upsilon(H_2O)$ stretching vibration and $\delta(H_2O)$ bending vibration of water molecules adsorbed in the product. The strong band at 513 cm^{-1} corresponds to the δ_{O-H} of hydroxyl groups. A small weak peak centered around 467 cm^{-1} is assigned to the Ni–O stretching mode [33–35]. Fig. 2b shows mixed characteristics of α-$Ni(OH)_2$ and β-$Ni(OH)_2$, in which the bands at about 656 and 513 cm^{-1} are characteristic of α-$Ni(OH)_2$ and β-$Ni(OH)_2$, respectively, consistent with the XRD result of Fig. 1b.

When increasing the volume ratio of EG to water in the mixed solvents to 1:1 and hydrothermally treated for 1.5 h (sample B1), the XRD peaks can be indexed to a single phase of α-$Ni(OH)_2$, as shown in Fig. 3a. However, when the hydrothermal time was increased to 3.5 h, a single phase of β-$Ni(OH)_2$ was obtained from the transformation of metastable α-$Ni(OH)_2$ intercalated by acetate ions and water (Fig. 3b, sample B2).

The XRD pattern of sample C1 (Fig. 4a) shows characteristic diffraction peaks of α-$Ni(OH)_2$ at 8.70, 4.35, 2.62 and 1.52 Å, respectively. Of these, the first two can be assigned to (0 0 l) (l = 1, 2). The reflections at 2.62 and 1.52 Å are both broad, with a sharp rise in intensity

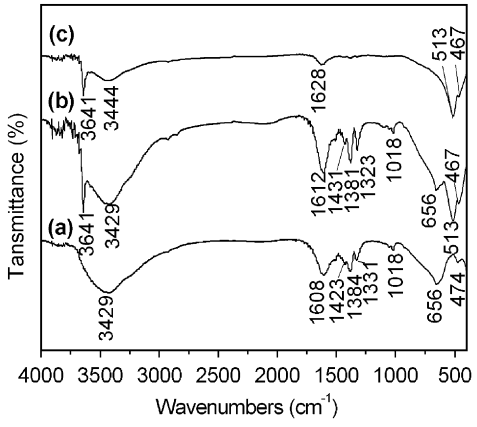

Fig. 2. FTIR spectra of samples: (a) sample A1; (b) sample A2; (c) sample A3.

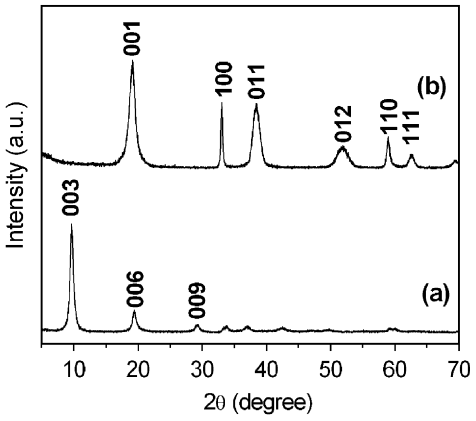

Fig. 3. XRD patterns of samples hydrothermally prepared using $Ni(CH_3COO)_2 \cdot 4H_2O$ in mixed solvents of EG and H_2O (volume ratio = 1:1) at 200 °C for different time: (a) sample B1; (b) sample B2.

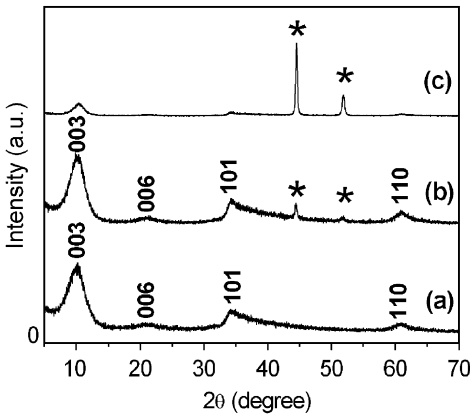

Fig. 4. XRD patterns of samples hydrothermally prepared using $Ni(CH_3COO)_2 \cdot 4H_2O$ in a single solvent of EG at 200 °C for different time: (a) sample C1; (b) sample C2; (c) sample C3 (the peaks labeled with asterisk (*) can be indexed to nickel).

followed by a pronounced asymmetry on the higher angle side. These "saw-tooth" reflections are typical of turbostratic phases which are ordered in two dimensions, but whose layers are orientationally disordered. They can be assigned to the two-dimensional (10) and (11) reflections, respectively. When the hydrothermal time was increased to 5.5 h (sample C2), a mixture of α-$Ni(OH)_2$ and nickel was formed (Fig. 4b). The formation of nickel indicates that further hydrothermal treatment of $Ni(CH_3COO)_2 \cdot 4H_2O$ in EG will result in the reduction of Ni^{2+} to Ni, which is further evidenced by sample C3 (Fig. 4c) in which nickel was formed as the main phase.

From the above XRD results, we can conclude that higher volume ratio of EG in the reaction system will reduce the interlayer spacing and enhance the stability of α-$Ni(OH)_2$. However, in the pure solution of EG, nickel was found as the reduction product. CH_3COO^- is a weak basic ion which tends to hydrolyze to form CH_3COOH and OH^- in aqueous solution. Therefore, we propose that $Ni(OH)_2$ is formed via the hydrolysis of CH_3COO^- ions

followed by the reaction between OH^- and Ni^{2+} ions. The presence of water is favorable for the hydrolysis of CH_3COO^- ions, leading to a more basic condition comparing with that without water. In this case, the transformation rate of α-$Ni(OH)_2$ to β-$Ni(OH)_2$ is accelerated by the more hydrolysis of CH_3COO^- ions. That is why for the same hydrothermal time, e.g., 1.5 h, a mixture of α-$Ni(OH)_2$ and β-$Ni(OH)_2$ was obtained at EG/H_2O ratio of 1:23, while only a single phase of α-$Ni(OH)_2$ was obtained at EG/H_2O ratio of 1:1. Although α-$Ni(OH)_2$ can form with different interlayer spacings, in fact, the previous literature reported that the amount of water and anions (CH_3COO^-) intercalated into the interlayers of α-$Ni(OH)_2$ could influence the value of the d spacings, which was influenced by the different physical and chemical properties of the solution when adjusting the content of EG. It is noted that the introduction of EG can adjust the interlayer spacing of unstable α-$Ni(OH)_2$, more EG will favor the stability of α-$Ni(OH)_2$ and at the same time reduce the interlayer spacing of the α-$Ni(OH)_2$, as evidenced in our experiments.

We also tried the experiments in which EG was substituted with ethanol. A single phase of α-$Ni(OH)_2$ was obtained, whose XRD pattern shows a diffraction peak at low angle around 0.9521 nm and a broad asymmetric band at about 0.2668 nm (Fig. 5a). When the hydrothermal time was increased to 1.5 h, the partial transformation of α-$Ni(OH)_2$ to β-$Ni(OH)_2$ occurred, indicating that α-$Ni(OH)_2$ is easier to transform to β-$Ni(OH)_2$ in ethanol aqueous solution than in equal volume EG aqueous solution, which was due to the different physical properties of ethanol from EG. β-$Ni(OH)_2$ formed when the hydrothermal time was 3.5 h or longer.

It is believed that the physical and chemical properties of the solvent can influence the solubility, reactivity, and diffusion behavior of the reagents and the intermediate [38,39]. In the present reaction system, the properties of the mixed solvents can be easily adjusted by controlling the volume ratio of EG or ethanol to water, since they have different physical properties, and hence different influence on the crystal phase. In fact, the formation of α-$Ni(OH)_2$ was stabilized by the intercalated CH_3COO^- ions and H_2O molecules. Different d value was caused by the different amount of the intercalated ions and H_2O molecules, which was influenced by the solution characteristics. As the hydrothermal time increased, the amount of intercalated ions and H_2O molecules decreased gradually, and finally α-$Ni(OH)_2$ supported by ions and H_2O molecules collapsed as a result of the formation of β-$Ni(OH)_2$.

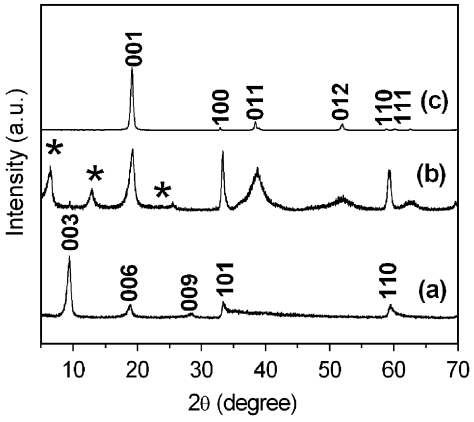

Fig. 5. XRD patterns of samples hydrothermally prepared using $Ni(CH_3COO)_2 \cdot 4H_2O$ in mixed solvents of ethanol and H_2O (volume ratio = 1:1) at 200 °C for different time: (a) sample D1; (b) sample D2; (c) sample D3 (the peaks labeled with asterisk (*) can be indexed to α-$Ni(OH)_2$).

3.2. Microstructure evolution

The morphology and structure of the samples prepared for different hydrothermal time was characterized by TEM and SAED. Fig. 6a reveals that sample A1 consisted of irregularly shaped or curved nanosheets. Fig. 6b shows a hollow-core flower-like nanostructure with large-size nanosheets as the petals. Due to the thin thickness of the nanosheets, crumpled nanosheets were observed. By increasing the hydrothermal time to 1.5 h, dense flower-like nanostructures with sizes of several micrometers were observed, which were constructed with the organization of nanosheets. From the FESEM images of Fig. 6d and its inset, the thickness of nanosheets was about 30 nm estimated from standing nanosheets. However, further prolonging the hydrothermal time to 3.5 h, flower-like nanostructures vanished and only nanosheets were observed (Figs. 6e and f). The SAED pattern (inset of Fig. 6f) shows that the individual nanosheet was single-crystalline with thickness along [0 0 1] direction (*c*-axis of hexagonal β-$Ni(OH)_2$). The sizes of β-$Ni(OH)_2$ nanosheets prepared for 10.5 h were similar to those prepared for 3.5 h, as shown in Figs. 6e and g, indicating that the formation process was almost complete in 3.5 h. The formation of nanosheets was a general result of the layered structure of $Ni(OH)_2$.

The morphology of $Ni(OH)_2$ formed in mixed solvents of ethanol and water was investigated, as shown in Fig. 7. At the early stage (1 h), small nanosheets were obtained with a poorly crystallized structure (Figs. 7a and b). Sphere-like structures with sizes of about 1 μm were observed for the hydrothermal time of 1.5 h. From the magnified TEM image (Fig. 7d), one can see that the sphere consisted of organized nanosheets. Flower-like structures consisting of curved nanosheets were also obtained (Fig. 7e). The SAED pattern taken from a randomly selected individual sphere-like structure (inset of Fig. 7d) exhibits bright elongated dots rather than rings, indicating that it consisted of $Ni(OH)_2$ nanosheets with an oriented crystallographic axis along the [0 0 1] direction. This phenomenon was different from that of using EG as the solvent, and we suggest that in this process the formation of the spheres and flowers consisting of nanosheets was due to the oriented attachment mechanism. It is apparent that the solution environment can

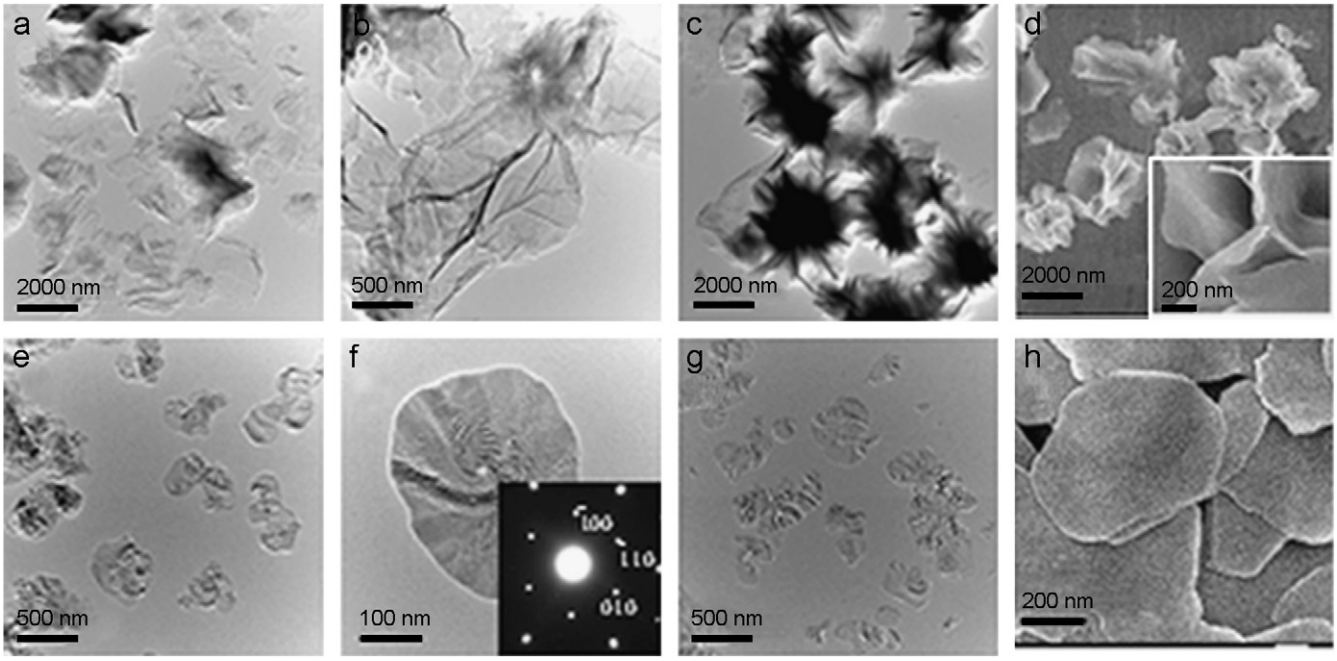

Fig. 6. TEM and FESEM images of samples hydrothermally prepared using $Ni(CH_3COO)_2 \cdot 4H_2O$ in 1 mL EG and 23 mL H_2O at 200 °C for different hydrothermal time: (a), (b) sample A1; (c), (d) sample A2; (e), (f) sample A3; (g), (h) sample A4.

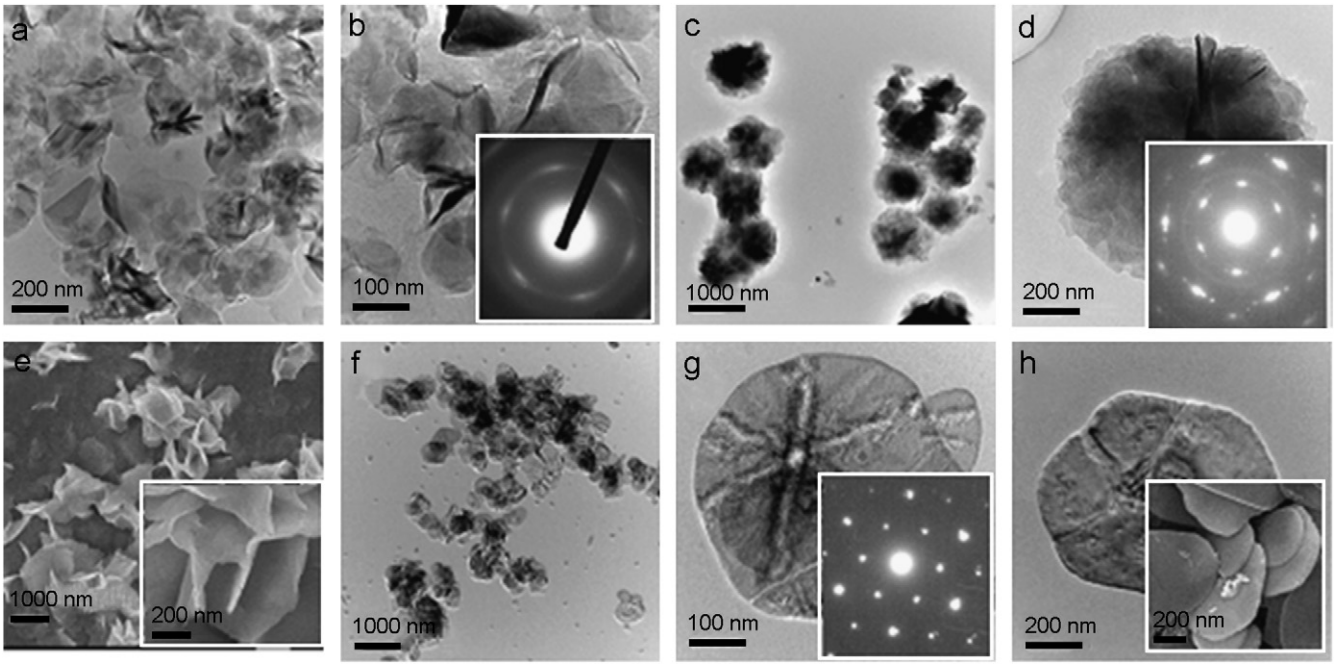

Fig. 7. TEM and FESEM images of samples hydrothermally prepared using $Ni(CH_3COO)_2 \cdot 4H_2O$ in the mixed solvents of ethanol and water at 200 °C for different time: (a), (b) sample D1; (c)–(e) sample D2; (f), (g) sample D3; (h) sample D4.

remarkably influence the growth of the particles. The nucleation and growth of crystals are strongly dependent on the properties of the solvent. The different morphology formed was due to the different physical and chemical properties of EG and ethanol, such as boiling point, dielectric constant, viscosity, polarity and surface tension. Further hydrothermal treatment of this kind of spheres and flowers, the nanosheets with the same orientation seemed to recrystallize into individual single-crystalline nanosheets, as revealed in Figs. 7f and g. The SAED pattern (inset of Fig. 7g) shows a single-crystalline nature of the nanosheet. Further increasing the hydrothermal time to 10.5 h, hexagonally shaped nanosheets were obtained (Fig. 7h).

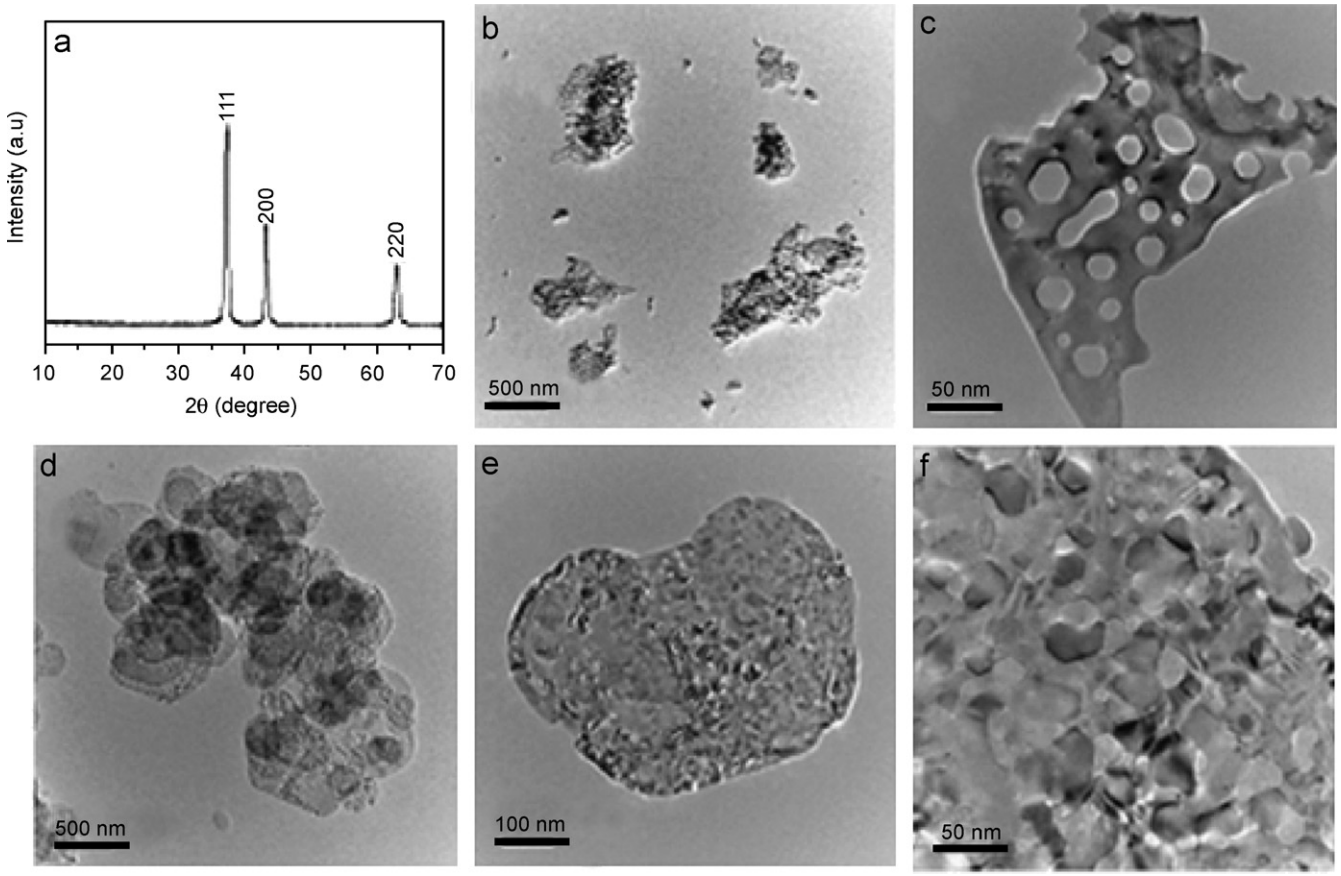

Fig. 8. (a) XRD patterns of sample E1; (b), (c) TEM images of sample E1; (d)–(f) TEM images of sample E2.

3.3. Thermal transformation from $Ni(OH)_2$ to NiO

The β-$Ni(OH)_2$ nanosheets as a precursor were thermally treated at 400 °C for 2 h in order to convert $Ni(OH)_2$ to NiO. The XRD pattern of sample E1 is shown in Fig. 8a, which can be indexed to a single phase of a cubic NiO (JCPDS No. 78-0643). No peaks from the precursor $Ni(OH)_2$ were observed in XRD pattern, indicating the complete transformation of $Ni(OH)_2$ to NiO. The TEM micrographs of two samples (E1 and E2) are presented in Figs. 8b–f. As for sample E1, the nanosheets were more irregular than the precursor $Ni(OH)_2$ nanosheets, and some nanosheet fragments were also observed. From a high-magnification image (Fig. 8c), one can see the presence of nanopores in the nanosheet. However, for the sample prepared using ethanol (sample E2), the size and shape of obtained NiO nanosheets were similar to those of the original β-$Ni(OH)_2$ nanosheets. The NiO sheet-like structure had no obvious go-through pores, which can be explained by the aggregation process of the nanosheets.

3.4. Cyclic voltammogram

Fig. 9 shows the typical cyclic voltammograms (CVs) of the β-$Ni(OH)_2$ nanosheets (samples A3 and D3) recorded at a scan rate of 10 mV/s in 6 M KOH solution vs. Hg/HgO reference electrode. The common feature on the CVs of β-$Ni(OH)_2$ nanosheets (Fig. 9) is that there are two partly overlapped oxidation current peaks of β-$Ni(OH)_2$ nanosheets located at the potential of about 450 and 520 mV, and one reduction current peak at the potential of about 320 mV. But these two oxidation current peaks did not occur at the first scan, for sample A3, these two oxidation current peaks appeared at the third scan, and vanished at the seventh scan. However, for sample D3, these two oxidation current peaks appeared at the third scan, and vanished at the fourteenth scan. This phenomenon indicates that new phase formed during the electrochemical cycling process, which changes the electrochemical reaction route, and the electrochemical process involves more reactions other than the mere oxidation process of Ni^{2+} to Ni^{3+}.

4. Conclusion

Nanosheets and flowers of nickel hydroxide (β-$Ni(OH)_2$ and α-$Ni(OH)_2$) have been synthesized using $Ni(CH_3COO)_2 \cdot 4H_2O$ in mixed solvents of ethylene glycol (EG) or ethanol and deionized water by a hydrothermal method at 200 °C for different time. The phases and morphologies of the obtained nickel hydroxide could be controlled by adjusting the experimental parameters such as

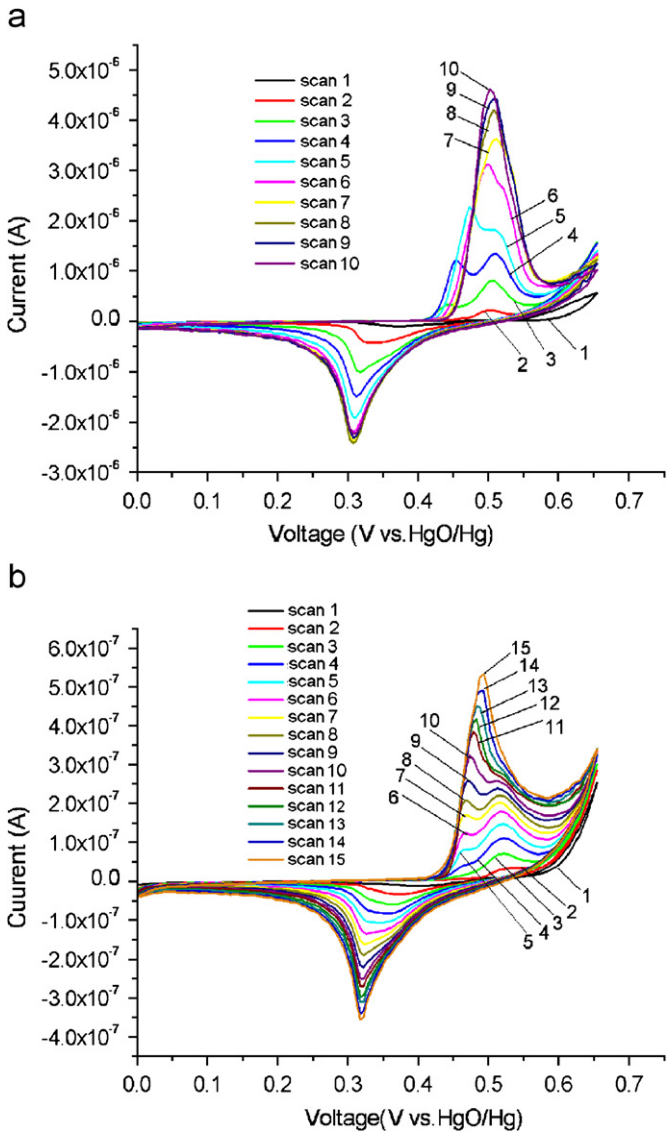

Fig. 9. Cyclic voltammograms of β-Ni(OH)$_2$ samples: (a) sample A3; (b) sample D3.

hydrothermal time and the volume ratio of water to EG or ethanol. Nanoporous nickel oxide nanosheets were obtained by heating nickel hydroxide in air at 400 °C. This method does not need any surfactant, and is simple, low cost and suitable for large-scale production of nanostructures of nickel hydroxide (β-Ni(OH)$_2$ and α-Ni(OH)$_2$) and nickel oxide.

Acknowledgments

Financial support from the National Natural Science Foundation of China (50472014) and The Chinese Academy of Sciences under the Program for Recruiting Outstanding Overseas Chinese (Hundred Talents Program) is gratefully acknowledged. We also thank the Fund for Innovation Research from The Shanghai Institute of Ceramics, The Chinese Academy of Sciences.

References

[1] C. Coudun, J.F. Hochepied, J. Phys. Chem.B 109 (2005) 6069.
[2] X.Y. Wang, H. Luo, P.V. Parkhutik, A.C. Millan, E. Matveeva, J. Power Sources 115 (2003) 153.
[3] S. Le Bihan, J. Guenot, M.C.R. Figlarz, Acad. Sci. Paris 270 (1970) 2131.
[4] J.J. Braconnier, C. Delmas, C. Fouassier, M. Figlarz, B. Beaudouin, P. Hagenmuller, Rev. Chim. Miner. 21 (1984) 496.
[5] B. Liu, X.Y. Wang, H.T. Yuan, Y.S. Zhang, D.Y. Song, Z.X. Zhou, J. Appl. Electrochem. 29 (1999) 855.
[6] I. Zhitomirsky, J. Appl. Electrochem. 34 (2004) 235.
[7] W.K. Hu, X.P. Gao, M.M. Geng, Z.X. Gong, D. Noréus, J. Phys. Chem. B 109 (2005) 5392.
[8] W.Y. Li, S.Y. Zhang, J. Chen, J. Phys. Chem. B 109 (2005) 14025.
[9] K. Matsui, T. Kyotani, A. Tomita, Adv. Mater. 14 (2002) 1216.
[10] F.S. Cai, G.Y. Zhang, J. Chen, X.L. Gou, H.K. Liu, S.X. Dou, Angew. Chem. Int. Ed. 43 (2004) 4212.
[11] S.L. Chou, F.Y. Cheng, J. Chen. Eur. J. Inorg. Chem. (2005) 4035.
[12] Z.H. Liang, Y.J. Zhu, X.L. Hu, J. Phys. Chem. B 108 (2004) 3488.
[13] D.N. Yang, R.M. Wang, M.S. He, J. Zhang, Z.F. Liu, J. Phys. Chem. B 109 (2005) 7654.
[14] D.N. Yang, R.M. Wang, J. Zhang, Z.F. Liu, J. Phys. Chem. B 108 (2004) 7531.
[15] Y. Wang, Q.S. Zhu, H.G. Zhang, Chem. Commun. (2005) 5231.
[16] D.B. Wang, C.X. Song, Z.S. Hu, X. Fu, J. Phys. Chem. B 109 (2005) 1125.
[17] D.L. Chen, L. Gao, Chem. Phys. Lett. 405 (2005) 159.
[18] H.B. Zhou, Z.T. Zhou, Solid State Ionics 176 (2005) 1909.
[19] Y.L. Zhao, J.M. Wang, H. Chen, T. Pan, J.Q. Zhang, C.N. Cao, Int. J Hydrogen Energy 29 (2004) 889.
[20] Y.P. Wang, J.W. Zhu, X.J. Yang, L.D. Lu, X. Wang, Thermochim. Acta 437 (2005) 106.
[21] I. Hotovy, J. Huran, L. Spiess, S. Hascik, V. Rehacek, Sensors Actuators B-Chem 57 (1999) 147.
[22] F.B. Zhang, Y.K. Zhou, H.L. Li, Mater. Chem. Phys. 83 (2004) 260.
[23] N.P. Duong, T. Satoh, M. Fiebig, Phys. Rev. Lett. 93 (2004) 117402.
[24] M. Ghosh, K. Biswas, A. Sundaresan, C.N.R. Rao, J. Mater. Chem. 16 (2006) 106.
[25] F. Li, H.Y. Chen, C.M. Wang, K.S. Hu, J. Electroanal. Chem. 531 (2002) 53.
[26] D.Y. Han, H.Y. Yang, C.B. Shen, X. Zhou, F.H. Wang, Powder Technol. 147 (2004) 113.
[27] C.K. Xu, K.Q. Hong, S. Liu, G.H. Wang, X.N. Zhao, J. Cryst. Growth 255 (2003) 308.
[28] Y.J. Zhan, C.R. Yin, C.L. Zheng, W.Z. Wang, G.H. Wang, J. Solid State Chem. 177 (2004) 2281.
[29] W.Z. Wang, Y.K. Liu, C.K. Xu, C.L. Zheng, G.H. Wang, Chem. Phys. Lett. 362 (2002) 119.
[30] J.H. Liang, Y.D. Li, Chem. Lett. 32 (2003) 1126.
[31] M.B. Zheng, J.M. Cao, Y.P. Chen, X.J. Ma, S.G. Deng, J. Tao, Chem. Lett. 34 (2005) 1174.
[32] W. Xing, F. Li, Z.F. Yan, H.M. Cheng, G.Q. Lu, Int. J. Nanosci. 3 (2004) 321.
[33] P.V. Kamath, G.N. Subbanna, J. Appl. Electrochem. 22 (1992) 478.
[34] G.J.D.A. Soler-Illia, M. Jobbagy, A.E. Regazzoni, M.A. Blesa, Chem. Mater. 11 (1999) 3140.
[35] X.M. Ni, Q.B. Zhao, B.B. Li, J. Cheng, H.G. Zheng, Solid State Commun. 137 (2006) 585.
[36] M. Rajamathi, P.V. Kamath, J. Power Sources 70 (1998) 118.
[37] H. Nishizawa, T. Kishikawa, H. Minami, J. Solid State Chem. 146 (1999) 39.
[38] Z.P. Liu, J.B. Liang, S. Li, S. Peng, Y.T. Qian, Chem. Eur. J. 10 (2004) 634.
[39] L.X. Yang, Y.J. Zhu, L. Li, L. Zhang, H. Tong, W.W. Wang, G.F. Cheng, J.F. Zhu. Eur. J. Inorg. Chem. (2006) 4787.